Computational evidence for structural consequences of Kiteplatin damage on DNA

Shaun T. Mutter,[a] Nicola Margiotta,[b] Paride Papadia,[c] and James A. Platts[a,*]

[a] School of Chemistry, Cardiff University, Park Place, Cardiff CF10 3AT (new address for Shaun)

[b] Department of Chemistry, University of Bari Aldo Moro, Via E. Orabona 4, 70125 Bari (Italy).

[c] Department of Biotechnology and Environmental Sciences, University of Salento, via Monteroni, 73100 Lecce (Italy)

* Author for correspondence:

Phone: +44-2920-874950 FAX: +44-2920-874030 Email: Platts@Cardiff.ac.uk

Abstract

The reaction of the potential anti-cancer drug kiteplatin, *cis*-[$PtCl_2$(*cis*-1,4-DACH)], with oligomers of single- and double-stranded DNA ranging from 2 to 12 base pairs in length was performed as a model for DNA interaction. The potential for conformational flexibility of single-stranded adducts was examined with density functional theory (DFT), and compared with data from ^{1}H-NMR 1D and 2D spectroscopy. This indicates the presence of multiple conformations of an adduct with d(GpG), but only one form of the adduct with d(TGGT). The importance of a suitable theoretical model, and in particular basis set, in reproducing experimental data is demonstrated. The DFT theoretical model was extended to platinated base pair step (GG/CC), allowing a comparison to the related compounds cisplatin and oxaliplatin. Adducts of kiteplatin with larger fragments of double-stranded DNA, including tetramer, octamer, and dodecamer, were studied theoretically using hybrid QM/MM methods. Structural parameters of all the base paired models were evaluated and binding energies calculated in gas phase and in solution; these are compared across the series, and also with the related complexes cisplatin and oxaliplatin, thus revealing insights into how kiteplatin binds to DNA, and similarities and differences between this and related compounds.

Keywords

cisplatin, kiteplatin, oxaliplatin, DNA structure, DFT, QM/MM

Introduction

Platinum complexes, such as the archetypal cisplatin (*cis*-[$PtCl_2(NH_3)_2$]), comprise one of the most widely used classes of anticancer drugs in the world. First synthesized in the nineteenth century, interest in cisplatin was sparked in the 1960s following Rosenberg's serendipitous discovery of cytotoxicity.[1] Marketed as Platinol, this is now widely used as an effective first line treatment for many cancers.[2] Despite this success, drawbacks associated with severe systemic toxicity have stimulated much interest in the development of improved platinum drugs, and in understanding the molecular mechanism that explains the biological activity of platinum compounds.[3,4] Such complexes show antitumour activity due to the formation of cytotoxic lesions on DNA with platinum adducts, preventing replication and eventually causing cell death.[5]

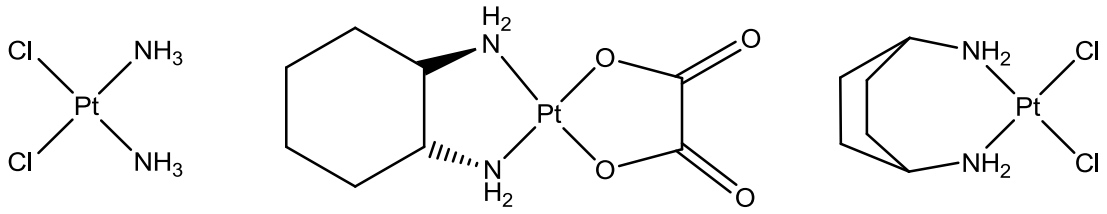

Figure 1 Structures of cisplatin (left), oxaliplatin (middle) and kiteplatin (right).

Oxaliplatin is a globally used alternative to cisplatin, and is not only better tolerated in the body but also displays a different spectrum of activity,[6] being particularly active against colorectal cancer.[7] This drug incorporates a 1*R*,2*R*-diaminocyclohexane (DACH) carrier group that is retained on binding to DNA, and is believed to facilitate transport into cells as well as formation of different DNA adducts than found with cisplatin. The origin and specific nature of these differences has been extensively studied, primarily by NMR spectroscopy.[8,9] It is believed that oxaliplatin forms fewer crosslinks than cisplatin at equimolar concentrations as adducts are bulkier and more hydrophobic, leading to different effects in the cell.[9,10]

The complex [$PtCl_2$(*cis*-1,4-DACH)], dubbed kiteplatin, contains an isomeric form of the oxaliplatin diamine ligand. Early studies indicated potency greater than cisplatin or oxaliplatin against several cell lines, and the potential for a different spectrum of activity

from those drugs.[11] Recently, activity against colon cancer cells that are resistant to conventional chemotherapy has been demonstrated.[12] Moreover, the unusual coordination geometry of kiteplatin, which contains a seven-membered chelate ring and large bite angle (ca. 97 °), leads to quite different conformational behaviour of complexes with free guanines or single-stranded DNA oligomers.[13] This feature might be correlated to the effectiveness of DNA-adducts of kiteplatin of blocking the Polη-catalyzed DNA synthesis.[14,15]

Experimental techniques such as NMR[9] and X-ray crystallography[16] can shed a great deal of light into the mode of action of such drugs, especially their interaction with DNA. Of particular relevance for the current work is a recent study that used ^{1}H and ^{31}P 1D and 2D NMR spectroscopy to determine conformations of kiteplatin's adducts with single-stranded DNA and their potential for interconversion.[17] Theoretical predictions from models based on quantum mechanics (QM), molecular mechanics (MM) or a combination of these (QM/MM) are increasingly used to complement such experiments.[18] A great many such studies have clarified and quantified various aspects of cisplatin's biochemistry, including the kinetics and thermodynamics of aquation and binding to DNA and other biological molecules, and the distortions induced in DNA on binding.[19,20,21,22,23] Similar studies of oxaliplatin and other alternatives have been reported, illuminating the similarities and differences between drugs.[24,25] Density functional theory (DFT) is the method of choice in almost all such studies, offering an excellent balance between accuracy and computational time and effort required. Properly chosen DFT methods correctly describe covalent and non-covalent bonding within platinum complexes and DNA, and between these species. However, such methods are typically applicable to a few hundred atoms with current computing, effectively limiting the size of DNA fragment to just two base pairs. Molecular mechanics (MM) methods are capable of describing much larger systems, and also to rapidly explore conformational freedom as in the recent study of cisplatin-TGG adducts,[23] but to date parameters are available only for cisplatin and oxaliplatin.

Recently, we set out hybrid QM/MM approaches for study of the interaction of platinum drugs with fragments of DNA from 2 to 12 base pairs, potentially including associated counterions and explicit solvent molecules. In this approach, platinum and ligands along with coordinated bases are treated with DFT, while the remainder of the DNA, counterions and solvent are treated with much more efficient MM methods. In our first study, the ability of

this approach to reproduce X-ray crystallographic and NMR structures of cisplatin with 2 and 8 DNA base pairs was tested, confirming the suitability of this approach.[26] A second study compared the binding of five drugs, including cisplatin and oxaliplatin, to octameric DNA, highlighting the importance of non-covalent as well as covalent interactions between drug and DNA and comparing the distortions induced by different drugs.[27] In this work, we apply DFT and QM/MM methods to kiteplatin-DNA complexes, with the twin goals of testing this approach against experimental NMR data, and subsequently discovering how the coordination geometry of kiteplatin affects binding and disruption of DNA.

Computational methods

DFT calculations were carried out using Gaussian09,[28] using the B97-D method[29] along with TZVP basis set,[30] taking advantage of the resolution of identity (RI) method. Solvated DFT calculations used the polarized continuum model (PCM) of aqueous phase.[31] QM/MM studies used the ONIOM method,[32] as implemented in Gaussian 09, with the high layer treated with BHandH/6-31+G**;[33] with SDD basis set and ECP on Pt, and the low layer with the AMBER (parm96.dat) forcefield.[34] In these calculations the QM layer includes Pt, ligand and the two coordinated guanines, while the MM layer is the remainder of the DNA fragment being studied, the sodium counterions, and any explicit water molecules present. For calculations on the QM layer the N9—C1' bond was broken and C1' replaced by hydrogen link atoms: see ref. 26 for further details. Optimisations were carried out using the GEDIIS algorithm,[35] and in some cases micro-iterations were also used. Relaxed potential energy scans were performed by freezing the torsion angle associated with 4 atoms centred on Pt-N7 bonds and relaxing all other coordinates, then varying the frozen torsion in steps of ±10°. This approach was previously validated against experimental data for complexes of various drugs with DNA oligomers.[27] In particular, comparison against NMR data for cisplatin complexes show that results do not depend strongly on parameters for the metal, since these cancel in the ONIOM expression. Calculation of binding energies in QM/MM models employed the polarizable continuum model (PCM) approach[36] after removal of explicit waters, using the cavity of the full system for all necessary calculations. Analysis of the resulting DNA structures was performed using X3DNA,[37] and exposed surface area calculated using MOLVOL.[38]

Results and Discussion

Adducts with single stranded DNA

The anticancer activity of cisplatin is triggered by the formation of adducts involving two adjacent guanines of DNA coordinated to the metal by their N7 atoms. The two cross-linked guanines adopt primarily a *Head-to-Head* (HH) arrangement with both G's having their H8 atoms on the same side of the platinum coordination plane. In contrast, the G bases adopt a *Head-to-Tail* (HT) arrangement in interstrand cross-links, which could also contribute to the anticancer activity.[39] Fast rotation, on the NMR time scale, about the Pt-N7 bonds in $Pt(G)_2$ adducts with untethered Gs greatly diminishes the informative potential of the NMR techniques when two ammines (such as in cisplatin) or a primary diamine are coordinated to platinum. The very large bite angle of *cis*-1,4-DACH in kiteplatin was exploited to diminish the dynamic motion and the interconversion between possible conformers. This was confirmed by the results obtained with the (*cis*-1,4-DACH)$Pt(5'\text{-}GMP)_2$ adduct, for which, at low temperature, three possible conformers (one HH and two HTs) were observed by ^{1}H-NMR.[13] Recent work showed that some or all of the four (2 HH and 2 HT; Scheme 1) possible conformers in adducts with single-stranded d(GpG) interconvert with a rate which is fast on the NMR time scale. Using a combination of variable temperature ^{1}H- and ^{31}P- and 2D-NMR spectroscopy, the dominant conformation was identified as HH1, with significant amounts of ΔHT1 at close to the physiological temperature (40 °C). Hence the *cis*-1,4-DACH ligand does not strongly influence the relative stability of conformers, but rather their interconversion rate due to the impeded rotation of the guanine bases with respect to the Pt-N7 bonds. This finding could be one of the reasons that may explain the difference in biological activity of kiteplatin as compared to that of cisplatin and oxaliplatin.

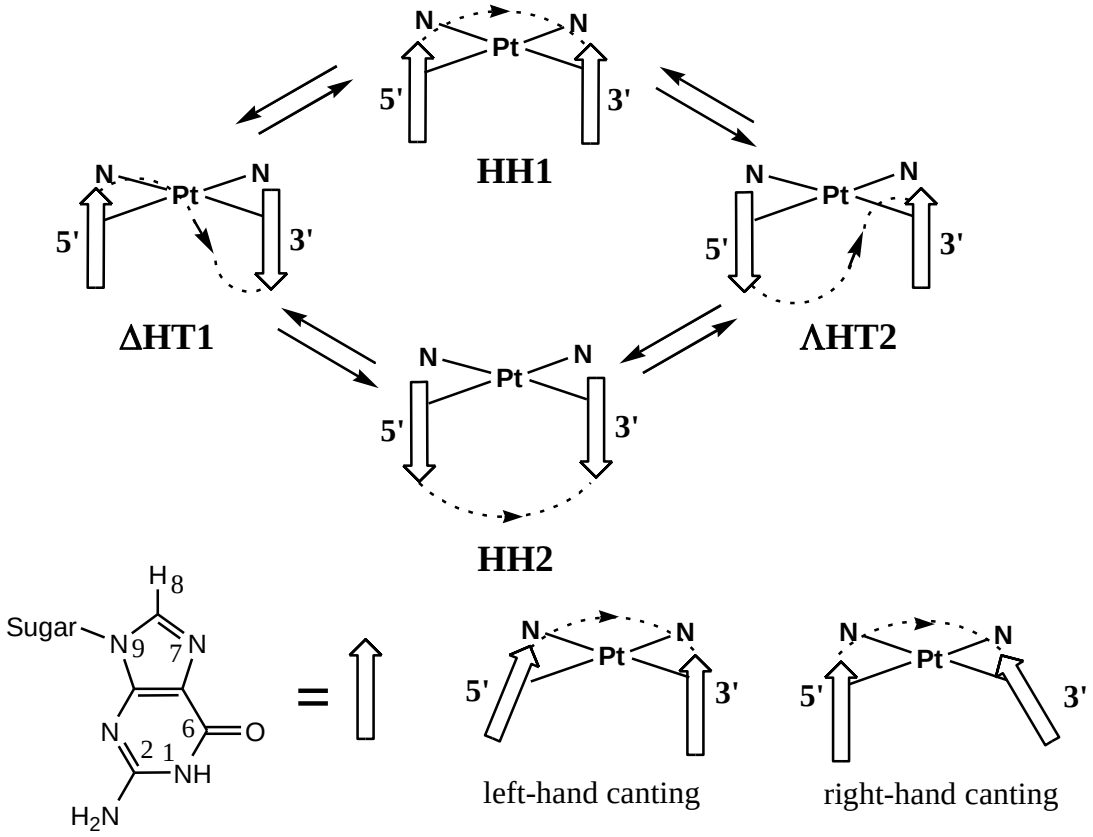

Scheme 1. Four possible conformers of adducts containing the Pt(dGpG) cross-link. The arrows represent the G bases while the phosphodiester backbone is represented by a curved dashed line linking the two arrows. Interconversion between conformers is possible via rotation about the Pt-G bonds. HT2 and HT1 differ, respectively, in the Λ and Δ handedness of GpG relative to the coordination plane. HH2 and HH1 differ, respectively, for the south or north orientation of the arrows representing the guanines, having placed 5'-G on the left- and 3'-G on the right-hand side. In the HH1 arrangement both Gs maintain the B-DNA *anti* conformation. Canting handedness is defined by two straight lines, one connecting the N7 atoms of the two coordinated guanines and the other overlapping the arrow representing a given guanine.

In order to examine the conformational preferences in kiteplatin-d(GpG) adduct, we turn to theoretical methods. We previously reported the use of MM methods to explore the conformational space of this adduct,[17] which located 54 conformations in total, with between 7 and 21 structures belonging to each family of conformers indicated in Scheme 1. Here, we employ DFT methods to obtain more reliable predictions, and also to examine the origin of

observed preferences in more detail. We first carried out geometry optimisation on all 54 complexes using a variety of DFT functionals, along with two relatively small basis sets, *i.e.* LANL2DZ,[40] and Stuttgart-Dresden ECP/basis set on Pt[41] with 6-31G(d)[42] on all other atoms. DFT methods tested included GGA (BLYP[43]), hybrid (B3LYP,[44] BHandH[45]), meta-hybrid (M06-2X[46]) and dispersion corrected (B97-D[47] and ω-B97x-D[48]). However, none of the methods tested were able to successfully identify any HH1 conformer as the global minimum, instead typically predicting a ΔHT1 form as having lowest energy. Therefore, we took the lowest energy structure from each family of conformers, and re-optimised using B97-D with the def2-TZVP basis set. As shown in Table 1, this larger basis set correctly predicts HH1 as the global energy minimum of this adduct in PCM calculation of aqueous phase (it should be noted that NMR experiments used a CD_3OD/D_2O mixture). HH2 and ΔHT1 forms lie within *ca.* 2 kcal/mol, while ΛHT2 is much higher in energy. Optimal geometries four conformers are shown in Figure 2.

Table 1 Relative energy (kcal mol^{-1}) and selected geometrical parameters (Å or °) calculated at B97-D/def2-TZVP level.

	HH1	HH2	ΔHT1	ΛHT2
Relative E	0.0	+1.37	+2.15	+5.63
Pt-N_L [a]	2.092	2.090	2.089	2.089
Pt-N_7 [a]	2.062	2.056	2.049	2.062
N_L-Pt-N_L	98.4	98.7	98.6	97.9
N7-Pt-N7	90.6	86.5	88.9	89.8
Dihedral [b]	83.4	47.4	61.4	59.7
C_8-N_7-Pt-N_L [c] 3'	112.2	-83.3	-130.3	128.0
5'	-130.4	136.5	-127.7	137.9
H_8...H_8	2.214	2.999	3.731	3.342
N_L-H_L...O_6 3'	2.380	3.915	1.967	1.941
5'	1.886	1.858	1.980	1.842

[a] Reported as the average of two unique values, that differ by less than 0.002 Å. [b] Angle between planes of six membered rings of the two guanines. [c] Torsion angle around Pt-DNA bond, defined relative to C8 in G and N in 1,4-DACH *cis* to N_7.

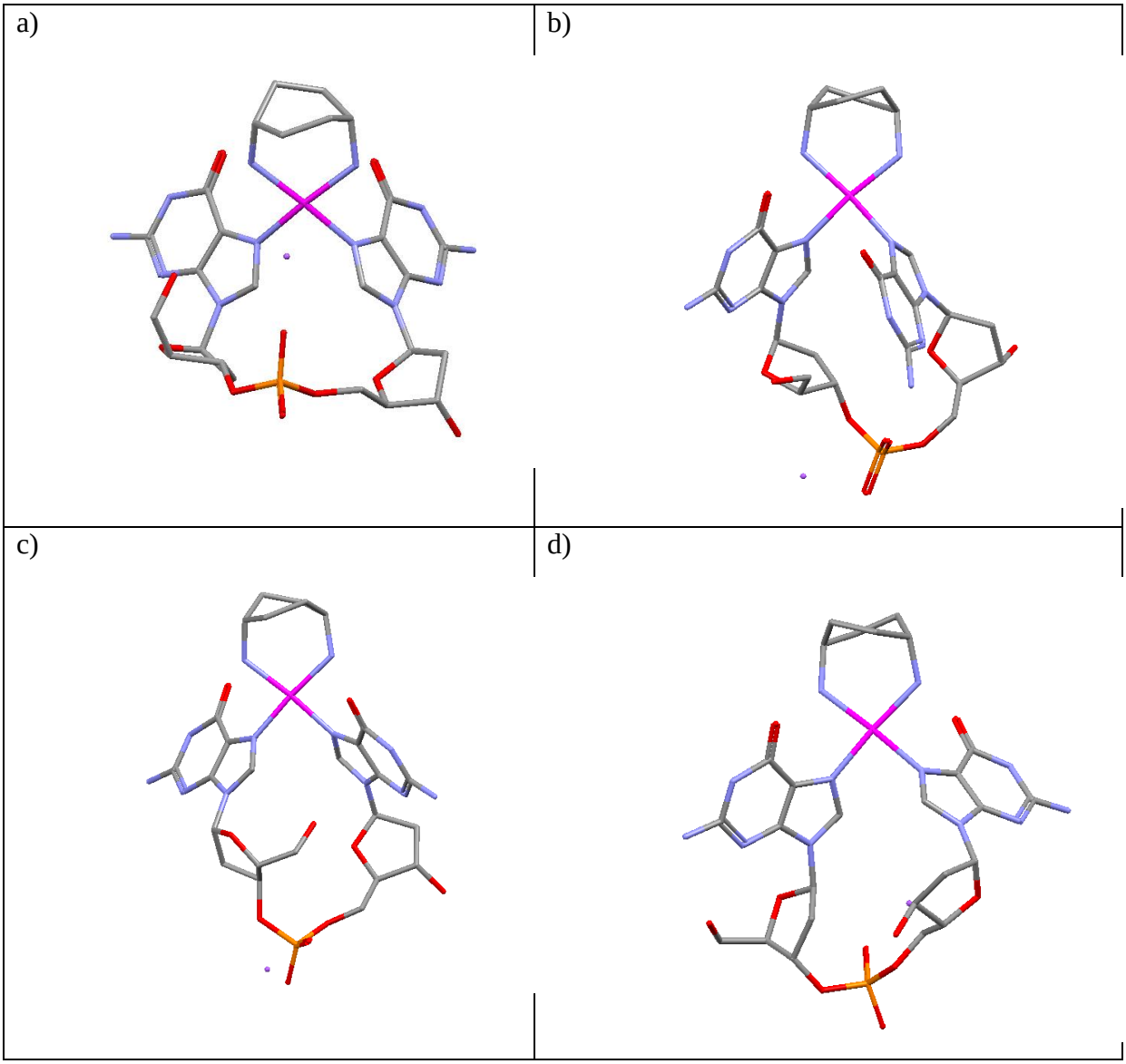

Figure 2 DFT optimised structures of 1,4-DACH-GpG adducts in a) HH1, b) HH2, c) ΔHT1 and d) ΛHT2 conformers.

Table 1 also contains selected geometrical parameters from these conformations. The platinum atom is coordinated in a square-planar mode to the *cis*-1,4-DACH ligand, thus giving rise to a large bite angle of *ca.* 98°. The remaining coordination sites are occupied by two guanine N7 atoms of the oligonucleotides, closing a 17-membered chelate ring. The greater flexibility of nucleotide coordination is evident in the greater range, almost 4°, of N7—Pt—N7 values observed. Other geometrical aspects of Pt coordination are largely as

expected, and rather similar to those calculated in similar manner for cisplatin.[26] For example, the mean planes of guanines in the HH1 conformer are almost orthogonal at 83°: the analogous value for HH1 cisplatin-d(GpG) conformer is 86.5°. It is notable, however, that hydrogen bonds between ligand NH_2 groups and base O6 can form despite the bulk of the 1,4-DACH ligand, and that this contact is typically shorter for 5' G than for 3'. This contrasts with our previous study of kiteplatin bound to double-stranded DNA, for which a strong H-bond to the 3' G was found, but no such interaction for 5' G.[12] We attribute this difference to the increased flexibility of the single-stranded oligomer considered here, which allows guanines to adopt orientations suitable for formation of such H-bonds. However, it is also apparent that H-bonding is unlikely to be the origin of the stability trend, since both HT conformers form two N—H…O H-bonds and the shortest such contact of all is found in the least stable structure. In the 2D-NMR study discussed above, the close contact observed between H8 nuclei was key to identifying the HH1 conformer: Table 1 shows that only this form exhibits a close contact between these nuclei. Other interesting information obtained by the analysis of the optimized HH1 (*cis*-1,4-DACH)Pt(d(GpG)) adduct (a in Figure 2) are puckering (N and S for 5'-G and 3'-G, respectively) and conformation (anti for both 5'-G and 3'-G) of the ribose base sugars which correspond to those revealed by the NMR investigation. In addition, both NMR data and computational investigation indicate a left-hand canting (canting handedness is defined in Scheme 1) of the 5'-G.[17]

To probe interconversion between isomers in more detail, we carried out relaxed potential energy scans for rotation about 3´ and 5´ Pt-N7 bonds, starting from the HH1 optimised geometry. These scans indicate approximate barriers of 10.5 and 18.5 kcal/mol for 3´ and 5´, respectively; thus we predict that formation of ΔHT1 is kinetically as well as thermodynamically favoured over ΛHT2. Moreover, Table 1 shows that the HH2 conformer is slightly lower in energy than the ΔHT1 one, such that one would expect to see more of the former than the latter if equilibrium between all species were established. However, NMR experiments show no sign of the HH2 form. We explain this apparent discrepancy by noting the likely barrier for formation of HH2 from either ΔHT1 or ΛHT2 is likely to involve a much higher barrier, since it requires the H8 atom of 5' guanine to occupy the same space as the aromatic rings of 3' guanine, or *vice versa* and so may not be accessible at experimental temperatures. Attempts at constructing potential energy scans for this process were unsuccessful, since the large forces induced gave unrealistic structures for which SCF

convergence failed. We cannot, therefore, estimate the barrier for formation of HH2 but this result supports chemical intuition that this conformer may not be accessible at temperatures used experimentally (0 – 40 °C).

The binding of damage-recognition proteins that control the signal-transduction pathways of cisplatin and oxaliplatin DNA adducts is highly dependent on the sequence context of the Pt-GG adduct. As an example, the DNA binding protein domain HMGB1a is able to bind to cisplatin-GG DNA adducts with much greater affinity than to oxaliplatin-GG DNA adducts in the TGGA sequence context, but presents much smaller differences in binding in the AGGC or TGGT sequence contexts.[10] Previous work has shown that the adduct of kiteplatin with 5'-d(TGGT)-3' results in a single conformer, assigned as having HH orientation of guanines. Starting from the HH1 structure of the (*cis*-1,4-DACH)Pt(d(GpG)) conformer, thymidines in B-DNA geometry were added to each guanine to form a single-stranded TGGT adduct and optimised at B97-D/6-31+G(d,p)-SDD level. Selected geometrical parameters are reported in Table 2, and DFT optimised structure is shown in Figure 3. Coordination geometry is similar to that obtained for the HH1 GpG adduct, as are H8···H8 and hydrogen bond distances: the former is sufficiently short to generate the NOE cross-peaks observed in the NMR NOESY spectrum.[17] However, the flanking effect of thymidines leads to a significant change in the orientation of guanines, which move closer to mutual planarity, with associated changes in Pt-N7 torsion angles. For this adduct, all attempts to generate alternative conformers by rotation about Pt—N bonds failed, such that we were only able to locate the HH1 form, in agreement with the NMR finding of single conformation.

Table 2 Selected geometrical parameters for kiteplatin-TGGT adduct (Å or °).

Pt-N_L [a]	2.096
Pt-N_7 [a]	2.076
N_L-Pt-N_L	97.8
N7-Pt-N7	86.4
Dihedral [b]	65.8
C_8-N_7-Pt-N_L 3'	89.4
5'	-133.1
H_8...H_8	2.667
N_L-H_L...O_6 3'	3.852
5'	1.844

[a] Reported as the average of two unique values. [b] Angle between planes of six membered rings of the two guanines. [c] Torsion angle around Pt-DNA bond, defined relative to C8 in G and N in 1,4-DACH *cis* to N_7.

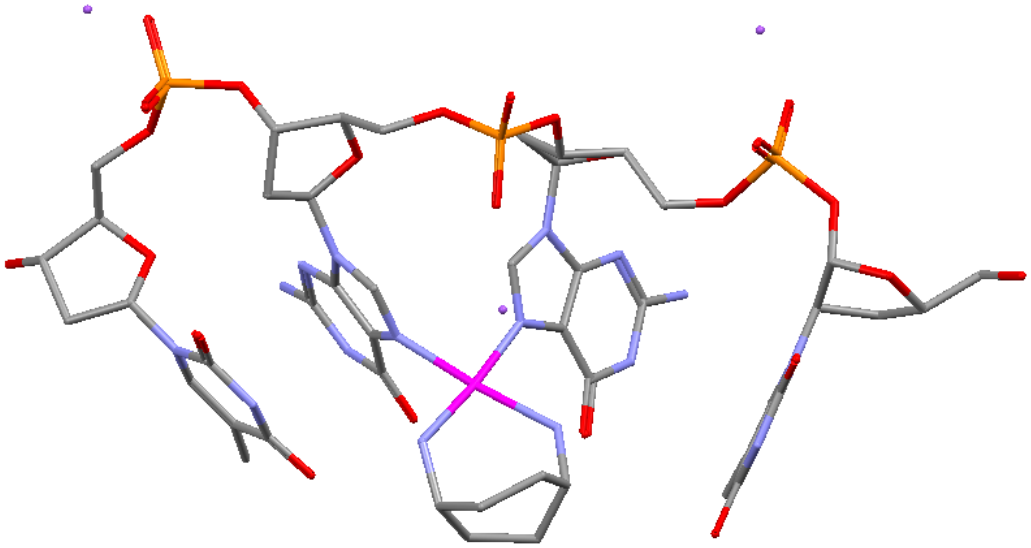

Figure 3 B97-D optimised structure of TGGT kiteplatin adduct. Hydrogens have been omitted for clarity.

Similarly to the case of HH1 (*cis*-1,4-DACH)Pt(d(GpG)) adduct, we compared the features of the optimized HH1 (*cis*-1,4-DACH)Pt(d(TGGT)) adduct (Figure 3) with data obtained by a

previous NMR investigation (puckering and conformation of the Gs ribose sugar and canting of the adduct). Once again, computed data correspond to experimental NMR data as evidenced by the puckering of the coordinated Gs (N and S for 5'-G and 3'-G, respectively) and by the conformation (anti for both 5'-G and 3'-G) of the ribose base sugars as well as the left-hand canting of the 5'-G.

Adducts with double stranded DNA

Adducts with double-stranded base pair step GG/CC were also constructed from PDB entry 1PGC, and optimisations carried out using B97-D, and optimised structure shown in Figure 4. Analysis of the resulting structures, as well as those for cisplatin and oxaliplatin adducts obtained previously,[27] was performed using X3DNA, with values reported in Table 3. Rise values show little change for the platinum adducts compared to free DNA, whereas shift and slide are markedly different to those in free DNA. The largest difference between the B-DNA and platinum adducts lies in roll values, which increase from –5.4° to approximately 28˚, with significant changes in twist but little difference in tilt angles. Coordination of the platinum to the two N7 sites on the adjacent guanines causes the roll angle to increase, presumably to relieve strain. All three platinum complexes give comparable results: kiteplatin has slightly smaller rise and less negative slide than the other drugs, but differences between drugs are rather small compared to the gross difference induced by platination of DNA.

Table 3 GG/CC base pair step parameters (Å and ˚).

	Shift	Slide	Rise	Tilt	Roll	Twist
Cisplatin	-1.39	-1.90	3.51	1.1	28.1	30.4
Oxaliplatin	-1.37	-1.93	3.54	1.0	28.1	31.2
Kiteplatin	-1.39	-1.78	3.46	1.1	27.9	28.7
B-DNA [a]	+0.10	+1.41	3.58	-1.1	-5.4	47.9

[a] Optimised at the same level, starting from canonical geometry.

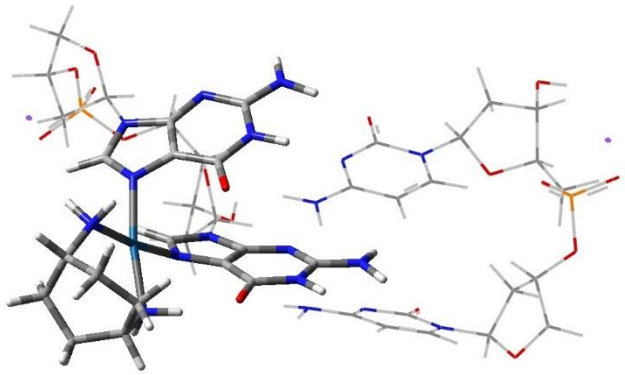

Figure 4 B97-D optimised structure of kiteplatin-GG/CC. Sugar phosphate backbone and CpC shown as wireframe for clarity.

As well as base-pair geometry, it is instructive to examine the geometry of the sugar phosphate backbone, as reported in Table 4. Gross differences of up to 40° between platinated and free DNA are evident in most backbone torsions, along with smaller changes between drugs. In most cases, cisplatin and oxaliplatin exhibit similar backbone torsions to one another, while kiteplatin differs from these by around 10°. However, there is no clear pattern on whether the kiteplatin complex is more distorted than the others: some torsion angles are further from their values in B-DNA, but others are closer than those found for cisplatin and oxaliplatin complexes.

Table 4 Backbone torsion parameters (˚).

	Cisplatin	Oxaliplatin	Kiteplatin	B-DNA [a]
α	-75.4	-75.3	-65.5	-36.0
β	-163.3	-163.7	-175.2	130.7
γ	48.0	47.6	56.6	57.1
χ [b]	-46.9	-55.4	-32.1	-91.8
χ [c]	9.6	-15.4	19.4	-107.1
δ	127.6	127.2	137.3	140.5
ε	167.3	-176.5	153.7	-153.2
ζ	-86.2	-86.1	-92.6	-169.9

[a] Optimised at the same level, starting from canonical geometry; [b] For the pentose sugar at the 3'end;

[c] For the pentose sugar at the 5' end.

Binding energies for the three complexes with GG/CC are reported in Table 5. In this data, oxaliplatin and kiteplatin are closely comparable in that their binding energies differ by less than 1 kcal/mol irrespective of solvent treatment. These two Pt drugs are isomers of each other and the binding energies suggest that differences in structure have little significance on binding. COSMO binding energies show a smaller range than gas phase, with the difference between weakest and strongest bound changing to 7.6 kcal/mol from 34.1 kcal/mol.

Table 5 B97-D counterpoise corrected binding energies to GG/CC (kcal/mol).

	Gas Phase Binding Energy	COSMO Binding Energy
Cisplatin	-283.9	-129.6
Oxaliplatin	-250.0	-122.6
Kiteplatin	-249.8	-122.0

The systems considered so far are the largest that can feasibly be studied using DFT on our available computing resources. Larger fragments of DNA, as well as explicit consideration of solvent molecules, require use of multilayer QM/MM techniques. By treating the areas of the molecule that are of greatest interest, in this case the platinum drug and the directly coordinated nucleobases, with QM methods and the remainder of the system with MM, calculations can be carried out on much larger and therefore more realistic biological systems. The chosen methodology to achieve this has recently been outlined by Gkionis and Platts,[26] for optimisation of analogous systems containing cisplatin and explicit water molecules. It can be difficult to achieve a fully optimised structure, since large molecules have many degrees of freedom and flat potential energy surfaces. To overcome this, optimisations were carried out in stages, with parts of the molecule frozen while others were free to move. By optimising parts at a time the forces for those can be reduced while maintaining the general structure from the initial construction of the coordinates, allowing efficient optimisation of complexes containing over one thousand atoms.

An adduct of kiteplatin with double stranded 5'-d(TG*G*T)-3'•5'-d(ACCA)-3', where * indicates the site of platination, was constructed from PDB entry 1AU5 by truncation of DNA and manual conversion to 1,4-DACH, retaining the positions of platinum and nitrogen atoms. Sodium counterions were manually placed in the vicinity of each phosphate group.

Initial optimisation allowed only the drug and central base pair step to relax, while coordinates of outer thymines and all backbone atoms were frozen, and proceeded smoothly. Subsequent optimisation of the entire structure with micro-iterations proved unsuccessful, resulting in separated DNA strands. Without use of microiterations, the geometry of the entire adduct could be optimised using the GEDIIS algorithm, leading to the structure shown in Figure 5.

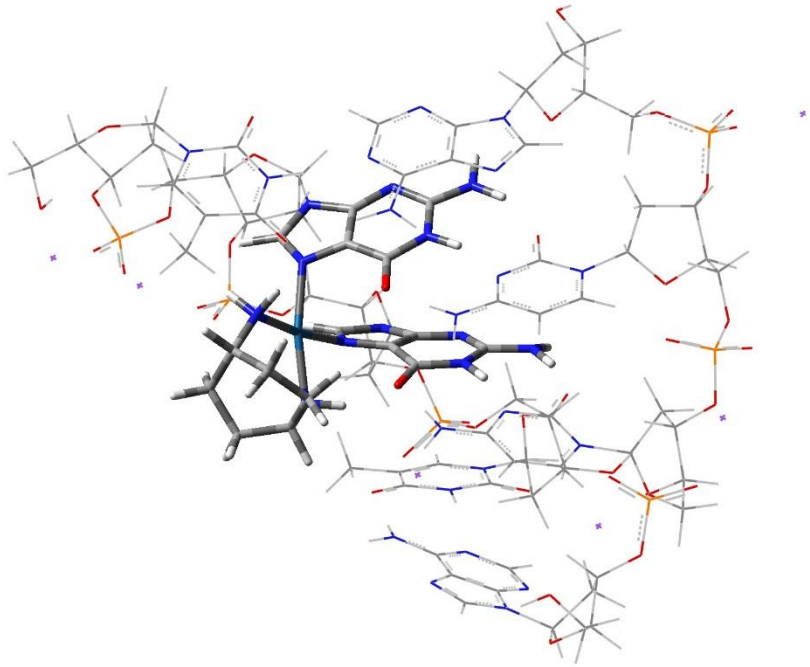

Figure 5 Optimised structure of kiteplatin tetramer, optimised using ONIOM BHandH/AMBER. MM layer is shown as wireframe for clarity.

Base pair parameters for this tetramer adduct are reported in Table 6, from which large deviation of the platinated base pair step from the flanking steps can be observed. This is most prevalent for the roll parameter, where the platinated bases result in a roll value significantly greater than for the remaining steps, or indeed the typical value in free DNA (Table 3). Twist and tilt parameters show large decreases for the central base pair step compared to the outer steps, whilst shift, slide, and rise are more comparable across the entire adduct.

Table 6 Base pair parameters for kiteplatin duplex-TGGT optimised in the gas phase (Å or °).

	Shift	Slide	Rise	Tilt	Roll	Twist
TG/CA	0.24	-1.98	2.78	9.9	6.3	30.0
GG/CC	0.86	-1.33	2.73	-5.5	19.3	22.9
GT/AC	0.89	-2.50	3.63	7.0	5.6	39.9

The double-stranded octamer of sequence (5'-d(CCTG*G*TCC)-3'•5'-d(GGACCAGG)-3') is of particular interest here, since an NMR structure (PDB entry 1AU5) of its cisplatin complex has been reported and hence was studied in detail when testing the QM/MM method employed. The NMR structure of the cisplatin octamer adduct was manually converted into 1,4-DACH, sodium counterions were placed in the vicinity of each phosphate group, and a water soak was carried out on the system to give a solvation shell of approximately 100 water molecules, using MOE. Following a similar procedure to that used for the tetramer, the first step successfully optimised the central base pair step and kiteplatin. Subsequently, the entire adduct was frozen and only water molecules optimised, then the MM region of DNA was optimised with central base pair step, kiteplatin, and water frozen. Only once all individual parts had been separately relaxed was full optimisation attempted. However, even from this partially relaxed starting point use of micro-iterations was unsuccessful, leading to separated single strands of DNA. Even without micro-iterations the GEDIIS lead to "unwound" DNA, such that an intermediate set of optimisation cycles in Cartesian coordinates was deemed necessary.

Only after such preliminary optimisation could we reach a fully optimised structure using microiterations, which is shown in Figure 6, with details in Table 7. Once again, the large positive roll value and smaller twist angle mark out the platinated central GG/CC step from those on either side of it. In this larger adduct, however, the rise value of the platinated step is rather smaller than for the non-platinated ones, and markedly smaller than for any reported above. The values of rise and roll in Table 7 are also quite different from those found for cisplatin bound to the same octamer, whether from experiment (5.50 Å and 58.7°) or using analogous QM/MM methods to those employed here (4.97 Å and 48.0°), which may give some insight into the origins of kiteplatin's different spectrum of activity.

Table 7 Base pair parameters for kiteplatin octamer adduct (Å or ˚).

Step	Shift	Slide	Rise	Tilt	Roll	Twist
CC/GG	-0.55	-0.52	3.03	5.4	-2.3	32.4
CT/AG	0.66	-0.90	3.76	1.4	-1.1	41.0
TG/CA	-1.33	0.31	2.94	-0.3	-5.2	36.3
GG/CC	1.10	-0.99	2.80	-3.0	23.6	25.3
GT/AC	1.03	-1.14	3.71	13.9	5.3	47.2
TC/GA	0.39	-0.60	3.38	-3.5	7.8	29.8
CC/GG	0.17	-1.99	3.81	3.5	-7.7	35.7

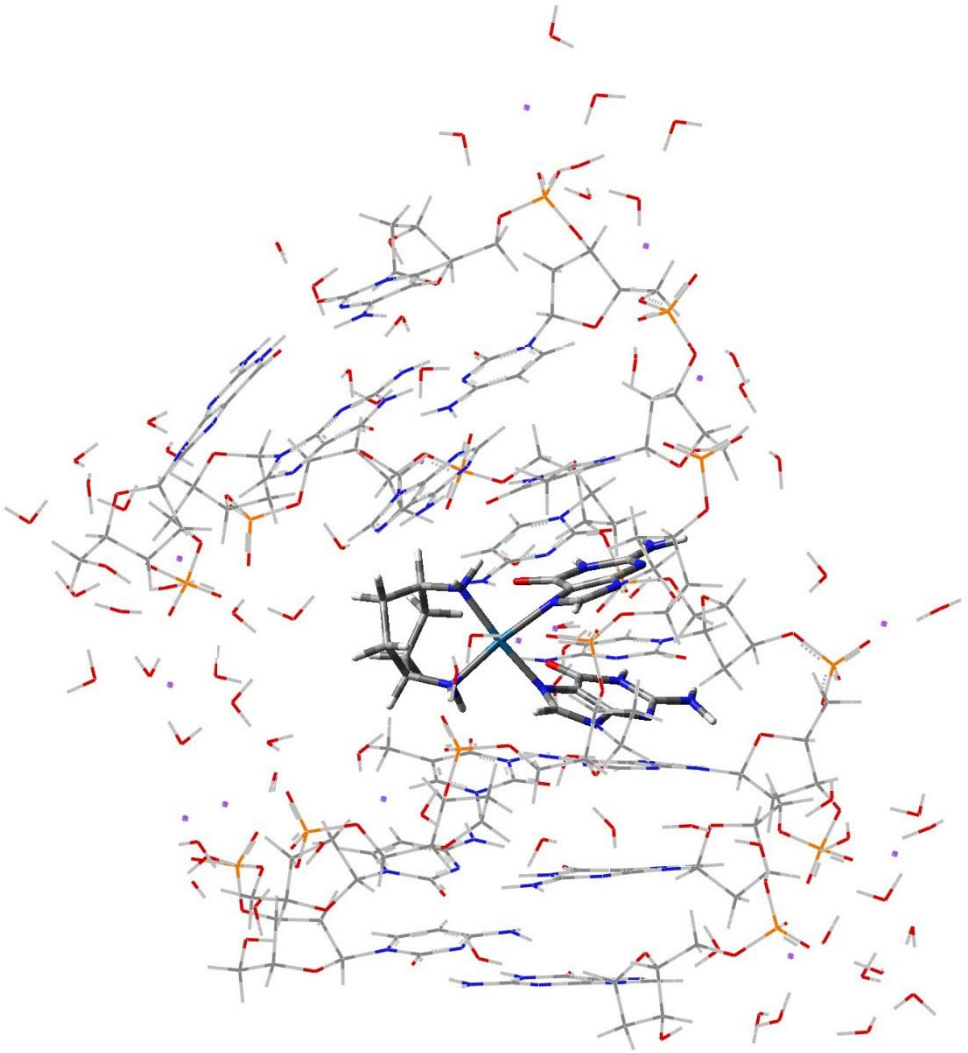

Figure 6 Optimised structure of kiteplatin octamer; MM layer shown as wireframe.

An adduct of kiteplatin with dodecameric DNA of sequence (5'-d(CCTCTG*G*TCTCC)-3'•5'-d(GGAGACCAGAGG)-3') was constructed from PDB entry 3LPV,[14] which contains oxaliplatin coordinated to the central GG/CC base pair step. The cyclohexane ring was converted into *cis*-1,4-DACH by hand and sodium counterions were placed in the vicinity of every phosphate moiety on the DNA backbone, in place of the mixed sodium and magnesium atoms present in the PDB structure. To solvate this adduct, a water soak was carried out using MOE to include approximately 100 explicit water molecules. The same optimisation method employed above was utilised, initially optimising just the platinum drug and the atoms in the coordinated base pair step. The explicit water molecules were then optimised with the remainder of the structure frozen, then MM atoms only optimised with water molecules and central base pair step frozen. The lowest energy structure was used as the starting point for full system optimisation in which all atoms are free to move. Once again, preliminary optimisation in Cartesian coordinates was necessary before full optimisation with GEDIIS and micro-iterations proved feasible. The optimised structure is shown in Figure 7, and details of this structure reported in Table 8. As expected, the central, platinated GG/CC step shows the greatest distortion compared to the remainder of the helix. This is especially prevalent in the roll parameter, which is significantly larger than reported above for the shorter DNA sequences. The shift value of the platinated base pair step is also notably larger than that for the remainder of the DNA helix.

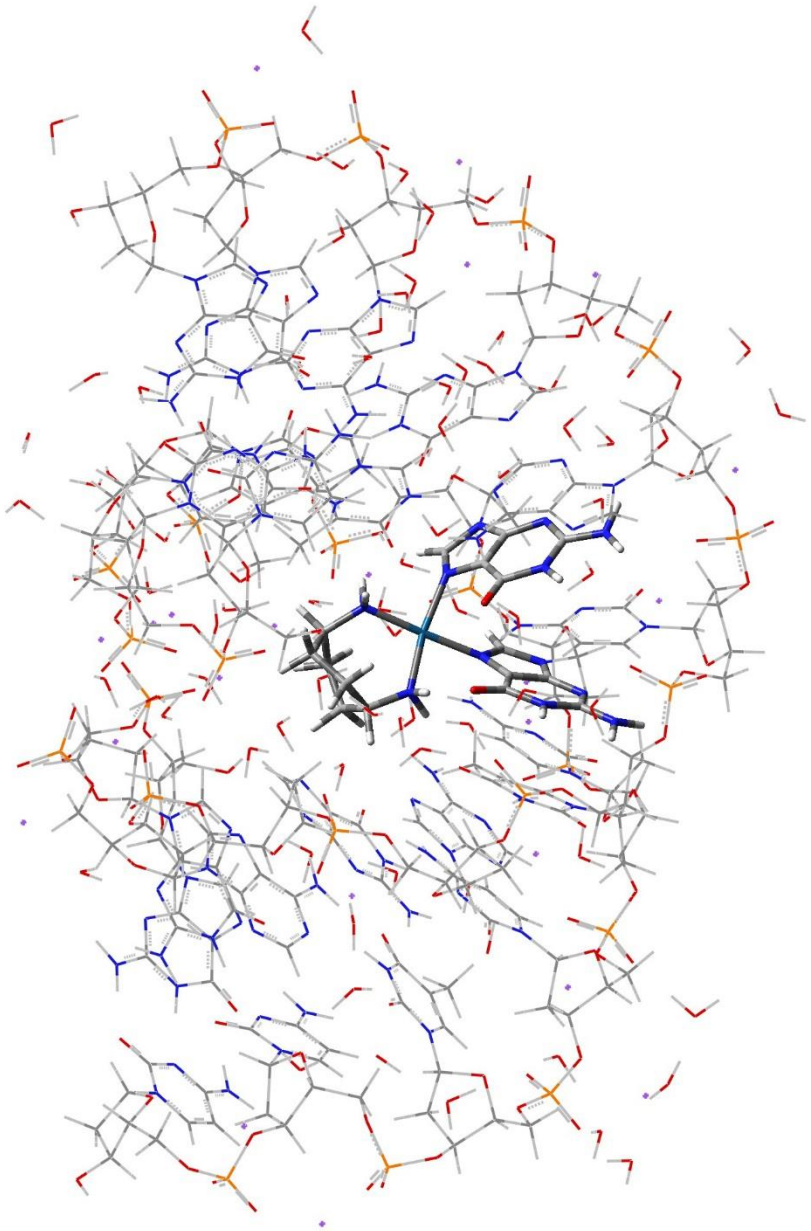

Figure 7 Optimised structure of kiteplatin dodecamer; MM layer shown as wireframe.

Table 8 Base pair parameters for kiteplatin dodecamer (Å or °).

	Shift	Slide	Rise	Tilt	Roll	Twist
CC/GG	-0.37	-2.06	3.16	1.2	7.5	26.7
CT/AG	0.20	-1.71	3.30	1.4	5.2	30.0
TC/GA	0.09	-1.95	3.28	-2.1	9.9	32.3
CT/AG	-0.14	-2.01	3.14	-0.2	4.8	31.5
TG/CA	-0.38	-1.38	2.92	4.1	8.1	27.1
GG/CC	1.16	-2.15	3.01	-2.4	34.8	30.2
GT/AC	-0.32	-1.03	3.06	3.1	8.6	33.9
TC/GA	1.11	-0.30	3.33	3.4	10.5	40.7
CT/AG	-0.31	-0.03	2.91	2.7	13.2	22.7
TC/GA	0.32	-1.26	4.34	-8.7	11.4	45.3
CC/GG	0.25	-0.10	2.86	3.1	-5.0	33.0

Comparison of adducts

A comparison of the base pair parameters of the platinated central GG/CC step for each adduct is shown in Figure 8. It is apparent that, as the size of the DNA fragment increases, some geometrical values change significantly, most notably in roll and twist which reach larger values in the larger adducts. The suitability of drawing conclusions from smaller model systems, such as just the central base pair step, is therefore called into question from this data. Figure 8 also displays a comparison of base pair step parameters across drugs and for B-DNA optimised in the same manner. The distortion of DNA caused by drug binding is broadly similar for each drug, with platination inducing positive shift, negative slide and much larger roll values in all cases. However, there are subtle differences between the drugs considered: in all values reported, kiteplatin is actually more similar to cisplatin, while oxaliplatin appears as the "odd one out" in this data.

Table 9 Geometrical parameters for kiteplatin-adduct with double stranded DNA (Å or °).

	Dimer	Tetramer	Octamer	Dodecamer
Pt-N_L [a]	2.040	2.037	2.041	2.029
Pt-N_7 [a]	2.029	2.030	2.020	2.042
N_L-Pt-N_L	99.2	99.8	96.4	96.6
N7-Pt-N7	84.2	86.1	84.4	86.5
C_8-N_7-Pt-N_L 3'	+140.1	+125.1	+113.3	+135.5
5'	-96.7	-101.8	-84.0	-80.8
H_8...H_8	2.944	3.417	3.418	3.323
N_L-H_L...O_6 3'	1.720	1.742	2.824	1.766
5'	3.361	3.213	3.878	3.808

[a] Reported as the average of two unique values. [b] Torsion angle around Pt-DNA bond, defined relative to C8 in G and N in 1,4-DACH *cis* to N_7.

Table 9 reports selected geometrical parameters regarding the coordination of kiteplatin to DNA fragments of different length. These data suggest that the adduct size has a negligible effect on the Pt-N bond lengths for both ligand and guanine base, while the longer adducts (octamer and dodecamer) exhibit a tightening of the angle N_L-Pt-N_L. For the N7-Pt-N7 angle, and the C_8-N_7-Pt-N_L torsions, the calculated values do not suggest any specific tendency. As expected, the H8...H8 distance is closer in the dimer, where the two guanines have no flanking bases enforcing stacking, while the distances stay reasonably similar for the tetramer, octamer, and dodecamer, reinforcing the idea that the addition of just two base pairs (3' and 5') is sufficient to restrict the mobility of the platinated guanines similarly to longer sequences. The hydrogen bonding distances H_L...O_6 are remarkably similar for the 3'G, with the exception of the octamer, around 1.7 Angstrom. The corresponding distance in 5'G, are very similar (about 3.3 Å) for the dimer and tetramer, while in the case of the octamer and dodecamer they are longer, around 3.8 Å, in both situations out of the acceptable range for hydrogen bonding.[49]

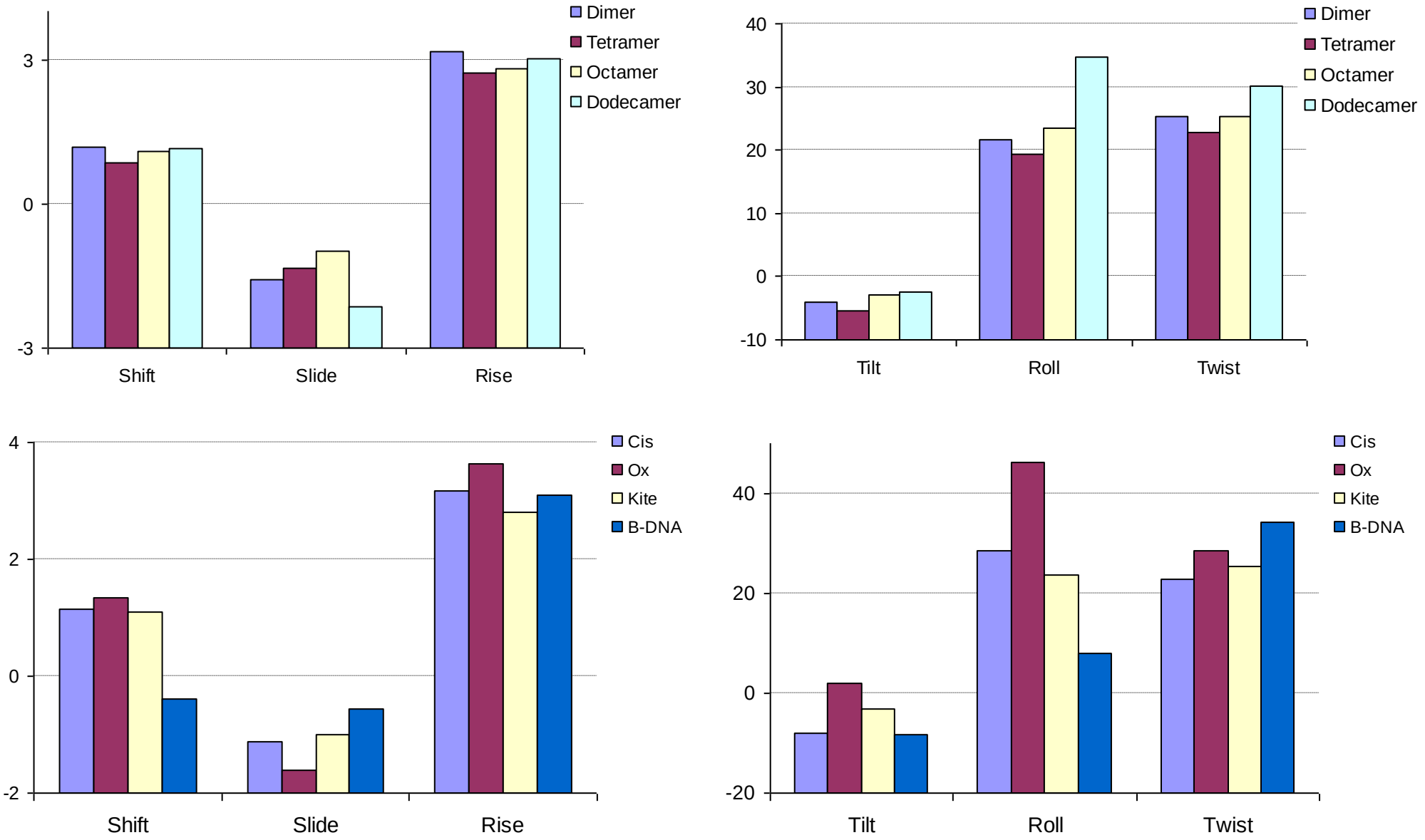

Figure 8 Geometry of platinated base-pair steps in different adducts: top row, kiteplatin bound to different DNA fragments; bottom: different drugs bound to octameric DNA: Cis = cisplatin, Ox = oxaliplatin, Kite = kiteplatin (Å or ˚).

Table 10 reports binding energies of kiteplatin to different DNA sequences, evaluated both in gas phase and simulated aqueous solvent. To calculate these values, explicit water molecules were removed from the systems, where present, and three single point energy calculations were carried out, on the platinum complex, the remainder of the DNA plus sodium counterions, and on the entire adduct. An implicit solvent model was chosen, instead of the already present explicit solvent molecules, to avoid the issue of assigning the water molecules in close proximity to the platinum to one of the two fragments. Gas phase values indicate that kiteplatin binds most weakly to the dimer, with a large increase to the tetramer and smaller increases for the octamer and dodecamer respectively. Aqueous phase data show a similar pattern, where the dimer is the weakest and binding becomes stronger as the size of the DNA adducts increase. In both cases, the dodecamer actually has slightly weaker binding than the octamer, but overall both series of values appear to converge as more bases are added. Kiteplatin's binding energy to octameric DNA lies between that reported previously for cisplatin (-245.4 kcal/mol in PCM water) and oxaliplatin (-299.6 kcal/mol), indicating that isomerisation of the DACH from 1,2 to 1,4 adversely affects binding somewhat, but that both isomers are more strongly bound than cisplatin.

Table 10 ONIOM binding energies of kiteplatin to DNA Adducts (kcal/mol).

	Gas Phase	PCM Aqueous
Dimer	-271.6	-33.8
Tetramer	-429.8	-186.0
Octamer	-473.5	-282.4
Dodecamer	-445.5	-277.2

The exposed surface areas of drug in complex with DNA are reported in Table 11. The dimer has the largest exposed area, presumably due to having the smallest DNA fragment, and as the DNA chain is extended the drug becomes more buried. The octamer has the lowest exposed area, whilst the dodecamer has a slightly higher value, similar to the pattern observed in binding energies. Once again, values apparently converge as the size of the DNA helix increases, which is what would be expected as the greater size of the DNA reduces the exposed surface of the drug. Comparisons to known drugs bound to octameric DNA show that kiteplatin is much more exposed to its environment than both cisplatin (63.2 $Å^2$) and slightly more so than oxaliplatin (117.1 $Å^2$). The data describing the environment of the platinum centre (Table 9), overall agree with the data regarding the binding energies (Table 10, PCM) and the exposed surface area (Table 11). The values for the dimer and tetramer are quite different, while much closer for the octamer and dodecamer, with the binding energy increasing with the decreasing exposed

area. Interestingly, the octamer has a lower PCM binding energy, and a lower exposed area than the dodecamer, which may give some insight into why the former is more strongly bound.

Table 11 Exposed surface area of kiteplatin in DNA complexes ($Å^2$).

	Exposed Area
Dimer	164.2
Tetramer	135.1
Octamer	120.7
Dodecamer	124.1

Conclusions

We have used theoretical calculations to probe the binding of kiteplatin to DNA, that, in some cases, had already been investigated by NMR experiments. Concerning single-stranded DNA oligomers, the dynamic behaviour of kiteplatin bound d(GpG), as revealed by NMR spectroscopy, is quite different from the one observed for cisplatin and its closest isomer currently used in therapy, oxaliplatin. The addition of bases to the model to form d(TGGT) globally slows the dynamic motion, showing a single conformer at room temperature. DFT calculations for the d(GpG) and d(TGGT) show that the main binding features at the platinum centre remain very similar (bonding distances, angles), with the only significant exception of the rotation of guanines around N7-Pt bond, a variation that can be attributed to the additional base-base interactions in the expanded sequence. As far as the structural features of the d(GpG)- and d(TGGT)-kiteplatin adducts concerns (puckering and conformation of the coordinated Gs ribose sugar and canting of the adduct), theoretical data confirm the NMR characterization previously performed on these compounds.

Adducts of kiteplatin with double-stranded DNA consisting of between 2 and 12 base pairs have also been examined theoretically, the larger cases requiring use of multilayer QM/MM methods that treat kiteplatin plus coordinate guanines with DFT and the remainder of the system with an atomistic forcefield. This approach allows us to calculate geometrical details associated with both coordination of Pt to guanine and the overall structure of DNA that results, as well as binding energy and exposed surface area of drug, comparing key quantities against other drugs. This analysis indicates that kiteplatin behaves more like cisplatin than oxaliplatin, despite being an isomer of the latter. However, kiteplatin and cisplatin DNA adducts differ markedly for the exposed surface area of the two drugs which is almost twofold higher in the case of kiteplatin. Since the bulk and shape of the carrier ligand in a Pt-based complex, as it projects out away from the DNA helix, will influence its interactions with nucleic acid

binding proteins or repair enzymes, we hypothesise that this peculiar feature of kiteplatin-DNA adducts could influence the markedly different pharmacological activity of this drug.

Acknowledgements

We acknowledge the University of Bari (Italy), the Italian Ministero dell'Università e della Ricerca (MIUR), the Fondo per gli investimenti della Ricerca di Base (FIRB RINAME RBAP114AMK), the European Union (COST CM1105, Functional metal complexes that bind to biomolecules), and the Inter-University Consortium for Research on the Chemistry of Metal Ions in Biological Systems (C.I.R.C.M.S.B.) for support.

References

[1] Rosenberg B, VanCamp L, Trosko JE, Mansour VH. Platinum compounds: a new class of potent antitumour agents. Nature 1969; 222: 385–386.

[2] Kelland, L. The resurgence of platinum-based cancer chemotherapy Nat. Rev. Chem. 2007; 7: 573-584.

[3] Wong, E Giandomenico, CM. Current status of platinum-based antitumor drugs. Chem. Rev. 1999; 99: 2451-2466.

[4] Galanski M, Jakupec MA, Keppler BK. Update of the preclinical situation of anticancer platinum complexes: novel design strategies and innovative analytical approaches Curr. Med. Chem. 2005;12:2075-2094.

[5] van Zutphen S, Reedijk J. Targeting platinum anti-tumour drugs: Overview of strategies employed to reduce systemic toxicity Coord Chem Rev 2005; 249: 2845–2853.

[6] Raymond E, Chaney SG, Taamma A, Cvitkovic E. Oxaliplatin: a review of preclinical and clinical studies. Ann Oncol. 1998;9:1053-1071.

[7] Díaz-Rubio E, Sastre J, Zaniboni A, Labianca R, Cortés-Funes H, de Braud F, Boni C, Benavides M, Dallavalle G, Homerin M. Oxaliplatin as single agent in previously untreated colorectal carcinoma patients: a phase II multicentric study. Ann Oncol. 1998;9:105-108.

[8] Wu Y, Pradhan P, Havener J, Boysen G, Swenberg JA, Campbell SL, Chaney SG. NMR solution structure of an oxaliplatin 1,2-d(GG) intrastrand cross-link in a DNA dodecamer duplex. J Mol Biol. 2004;341:1251-1269.

[9] Wu Y, Bhattacharyya D, King CL, Baskerville-Abraham I, Huh SH, Boysen G, Swenberg JA, Temple B, Campbell SL, Chaney SG. Solution structures of a DNA dodecamer duplex with and without a cisplatin 1,2-d(GG) intrastrand cross-link: comparison with the same DNA duplex containing an oxaliplatin 1,2-d(GG) intrastrand cross-link. Biochemistry. 2007;46:6477-6487.

[10] Bhattacharyya D, Ramachandran S, Sharma S, Pathmasiri S, King CL, Baskerville-Abraham I, Boysen G, Swenberg JA, Campbell SL, Dokholyan NV, Chaney SG. Flanking bases influence the nature of DNA distortion by platinum 1,2-intrastrand (GG) cross-links PLoS ONE 2011, 6, e23582.

[11] Hoeschele JD, Showalter HD, Kraker AJ, Elliott WL, Roberts BJ, Kampf JW. Synthesis, structural characterization, and antitumor properties of a novel class of large-ring platinum(II) chelate complexes incorporating the cis-1,4-diaminocyclohexane ligand in a unique locked boat conformation. J Med Chem. 1994;37:2630-2636.

[12] Margiotta N, Marzano C, Gandin V, Osella D, Ravera M, Gabano E, Platts JA, Petruzzella E, Hoeschele JD, Natile G. Revisiting [PtCl2(cis-1,4-DACH)]: An Underestimated Antitumor Drug with Potential Application to the Treatment of Oxaliplatin-Refractory Colorectal Cancer J. Med. Chem. 2012; 55: 7182-7192.

[13] Ranaldo R, Margiotta N, Intini FP, Pacifico C, Natile G. Conformer distribution in (cis-1,4-DACH) bis(guanosine-5'-phosphate)platinum(II) adducts: a reliable model for DNA adducts of antitumoral cisplatin. Inorg Chem. 2008;47:2820-2830.

[14] Brabec V, Malina J, Margiotta N, Natile G, Kasparkova J. Thermodynamic and Mechanistic Insights into Translesion DNA Synthesis Catalyzed by Y-Family DNA Polymerase Across a Bulky Double-Base Lesion of an Antitumor Platinum Drug Chem. Eur. J. 2012; 18: 15439-15448.

[15] Kasparkova J, Suchankova T, Halamikova A, Zerzankova L, Vrana O, Margiotta N, Natile G, Brabec V. Cytotoxicity, cellular uptake, glutathione and DNA interactions of an antitumor large-ring Pt II chelate complex incorporating the cis-1,4-diaminocyclohexane carrier ligand. Biochem Pharmacol. 2010;79:552-564.

[16] Sherman SE, Gibson D, Wang AH, Lippard SJ. X-ray structure of the major adduct of the anticancer drug cisplatin with DNA: cis-[Pt(NH3)2(d(pGpG))]. Science. 1985;230:412-417.

[17] Margiotta N, Petruzzella E, Platts JA, Mutter ST, Deeth RJ, Ranaldo R, Papadia P, Marzilli PA, Marzilli LG, Hoeschele JD Natile G, DNA fragment conformations in adducts with Kiteplatin. Dalton Trans., 2014, in press (DOI 10.1039/c4dt01796j)

[18] Banáš P, Jurečka P, Walter NG, Šponer J,§ Otyepka M. Theoretical studies of RNA catalysis: Hybrid QM/MM methods and their comparison with MD and QM. Methods 2009; 49: 202–216.

[19] Basch H, Krauss M, Stevens WJ, Cohen D. Binding of $Pt(NH_3)_3^{2+}$ to nucleic acid bases. Inorg. Chem. 1985; 24: 3313–3317.

[20] Carloni P, Andreoni W, Hutter J, Curioni A, Giannozzi P, Parinello M. Structure and bonding in cisplatin and other Pt (II) complexes. Chem. Phys. Lett. 1995; 234: 50–56.

[21] Pavankumar PNV, Seetharamulu P, Yao S, Saxe JD, Reddy DG, Hausheer FH Comprehensive ab initio quantum mechanical and molecular orbital (MO) analysis of cisplatin: structure, bonding, charge density, and vibrational frequencies. J. Comput. Chem. 1999; 20: 365–382.

[22] Baik MH, Friesner RA, Lippard SJ Theoretical study of cisplatin binding to purine bases: why does cisplatin prefer guanine over adenine? J Am Chem Soc. 2003;125:14082-92.

[23] Monnet, J. and Kozelka, J. Cisplatin GG-crosslinks within single-stranded DNA: Origin of the preference for left-handed helicity J. Inorg. Biochem. 2012; 115: 106-112.

24 Sarmah, P. and Deka, R.C. Solvent effect on the reactivity of cis-platinum (II) complexes: A density functional approach. Int. J. Quantum Chem. 2008; 108: 1400–1409.

[25] Zhu C, Raber J, Eriksson LA. Hydrolysis process of the second generation platinum-based anticancer drug cis-amminedichlorocyclohexylamineplatinum (II). J. Phys. Chem. B 2005; 109: 12195–12205.

[26] Gkionis K, Platts JA Comp. QM/MM studies of cisplatin complexes with DNA dimer and octamer Theor. Chem. 2012; 993, 60-65.

[27] Gkionis K, Mutter S, Platts JA. QM/MM description of platinum–DNA interactions: comparison of binding and DNA distortion of five drugs. RSC Advances 2013; 3: 4066-4013.

[28] Gaussian 09, Revision C.01, M. J. Frisch, G. W. Trucks, H. B. Schlegel, G. E. Scuseria, M. A. Robb, J. R. Cheeseman, G. Scalmani, V. Barone, B. Mennucci, G. A. Petersson, H. Nakatsuji, M. Caricato, X. Li, H. P. Hratchian, A. F. Izmaylov, J. Bloino, G. Zheng, J. L. Sonnenberg, M. Hada, M. Ehara, K. Toyota, R. Fukuda, J. Hasegawa, M. Ishida, T. Nakajima, Y. Honda, O. Kitao, H. Nakai, T. Vreven, J. A. Montgomery, Jr., J. E. Peralta, F. Ogliaro, M. Bearpark, J. J. Heyd, E. Brothers, K. N. Kudin, V. N. Staroverov, T. Keith, R. Kobayashi, J. Normand, K. Raghavachari, A. Rendell, J. C. Burant, S. S. Iyengar, J. Tomasi, M. Cossi, N. Rega, J. M. Millam, M. Klene, J. E. Knox, J. B. Cross, V. Bakken, C. Adamo, J. Jaramillo, R. Gomperts, R. E. Stratmann, O. Yazyev, A. J. Austin, R. Cammi, C. Pomelli, J. W. Ochterski, R. L. Martin, K. Morokuma, V. G. Zakrzewski, G. A. Voth, P. Salvador, J. J. Dannenberg, S. Dapprich, A. D. Daniels, O. Farkas, J. B. Foresman, J. V. Ortiz, J. Cioslowski, and D. J. Fox, Gaussian, Inc., Wallingford CT, 2010.

[29] Grimme S. Semiempirical GGA-type density functional constructed with a long-range dispersion correction J. Comp. Chem. 2006; 27: 1787-99.

[30] Weigend F, Ahlrichs R. Balanced basis sets of split valence, triple zeta valence and quadruple zeta valence quality for H to Rn: Design and assessment of accuracy. Phys. Chem. Chem. Phys. 2005; 7: 3297-3305.

[31] Klamt A, Schuurmann G.COSMO: A new approach to dielectric screening in solvents with explicit expressions for the screening energy and its gradient. J. Chem. Soc, Perkin Trans. 2 1993: 799-805.

[32] Vreven T, Byun KS, Komáromi I, Dapprich S, Montgomery Jr JA, Morokuma K, Frisch MJ. Combining quantum mechanics methods with molecular mechanics methods in ONIOM. J. Chem. Theory Comput. 2006; 2: 815-26.

[33] Ditchfield R, Hehre WJ, Pople JA. Self-Consistent Molecular Orbital Methods. 9. Extended Gaussian-type basis for molecular-orbital studies of organic molecules. J. Chem. Phys., 1971; 54: 724-729.

[34] Cornell WD, Cieplak P, Bayly CI, Gould IR, Merz Jr KM, Ferguson DM, Spellmeyer DC, Fox T, Caldwell JW, Kollman PA. A second generation force-field for the simulation of proteins, nucleic-acids, and organic-molecules. J. Am. Chem. Soc., 1995; 117: 5179-97.

[35] Li X, Frisch MJ. Energy-represented DIIS within a hybrid geometry optimization method. J. Chem. Theory Comput., 2006; 2: 835-39.

[36] Barone V, Cossi M. Quantum calculation of molecular energies and energy gradients in solution by a conductor solvent model. J. Phys. Chem. A, 1998; 102: 1995-2001.

[37] http://w3dna.rutgers.edu/, accessed 1st Nov 2013

[38] Dodd LR, Theodorou DN. Analytical treatment of the volume and surface area of molecules formed by an arbitrary collection of unequal spheres intersected by planes. Mol. Phys. 1991; 72: 1313-1345.

[39] Natile G, Marzilli LG. Non-covalent interactions in adducts of platinum drugs with nucleobases in nucleotides and DNA as revealed by using chiral substrates. Coord. Chem. Rev. 2006; 250: 1315-1331.

[40] Hay PJ, Wadt WR, Ab initio effective core potentials for molecular calculations - potentials for the transition-metal atoms Sc to Hg. J. Chem. Phys., 82 (1985) 270-83.

[41] Andrae D, Haeussermann U, Dolg M, Stoll H, Preuss H, Energy-adjusted ab initio pseudopotentials for the 2nd and 3rd row transition-elements. Theor. Chem. Acc., 77 (1990) 123-41.

[42] a) Ditchfield R, Hehre WJ, Pople JA, Self-Consistent Molecular Orbital Methods. 9. Extended Gaussian-type basis for molecular-orbital studies of organic molecules. J. Chem. Phys., 54 (1971) 724; b) Hehre WJ, Ditchfield R, Pople JA, Self-Consistent Molecular Orbital Methods. 12. Further extensions of Gaussian-type basis sets for use in molecular-orbital studies of organic-molecules. J. Chem. Phys., 56 (1972) 2257; c) Hariharan PC, Pople JA, Influence of polarization functions on molecular-orbital hydrogenation energies Theor. Chem. Acc., 28 (1973) 213-22.

[43] a) Becke AD, Density-functional exchange-energy approximation with correct asymptotic-behavior, Phys. Rev. A, 38 (1988) 3098-100; b) Lee C, Yang W, Parr RG, Development of the Colle-Salvetti correlation-energy formula into a functional of the electron density, Phys. Rev. B, 37 (1988) 785-89.

[44] Becke AD, Density-functional thermochemistry. III. The role of exact exchange J. Chem. Phys., 98 (1993) 5648-52.

[45] Becke AD, A new mixing of Hartree-Fock and local density-functional theories J. Chem. Phys., 98 (1993) 1372-77.

[46] Zhao Y, Truhlar DG, The M06 suite of density functionals for main group thermochemistry, thermochemical kinetics, noncovalent interactions, excited states, and transition elements: two new functionals and systematic testing of four M06-class functionals and 12 other functionals Theor. Chem. Acc., 120 (2008) 215-41.

[47] Grimme S, Semiempirical GGA-type density functional constructed with a long-range dispersion correction J. Comp. Chem., 27 (2006) 1787-99.

[48] Chai JD, Head-Gordon M, Long-range corrected hybrid density functionals with damped atom-atom dispersion corrections Phys. Chem. Chem. Phys., 10 (2008) 6615-20.

[49] Arunan E, Desiraju GR, Klein RA, Sadlej J, Scheiner S, Alkorta I, Clary DC, Crabtree RH, Dannenberg JJ, Hobza P, Kjaergaard HG, Legon AC, Mennucci B, Nesbitt DJ. Defining the hydrogen bond: An account. *Pure Appl. Chem.* 2011; **83**: 1619–1636.